EDITOR
Prof. Dr. E. Nihal ERCAN

Research and Evaluations in the Field of

PHYSICS

June 2025

Privilege Holder • Yaşar Hız
Editor-in-chief • Eda Altunel
Prepared for Publication • Gece Kitaplığı
Editor • Prof. Dr. E. Nihal ERCAN

First Edition • June 2025 / ANKARA

ISBN • 978-625-388-438-3

Gece Kitaplığı
Adress: Kızılay Mah. Fevzi Çakmak 1. Sokak Ümit Apt
No: 22/A Çankaya/ANKARA Tel: 0312 384 80 40

www.gecekitapligi.com
gecekitapligi@gmail.com

Printing and Binding
Bizim Buro
Certificate No: 42488

Research And Evaluations In The Field Of Physics

June 2025

Editor:
Prof. Dr. E. Nihal ERCAN

CONTENTS

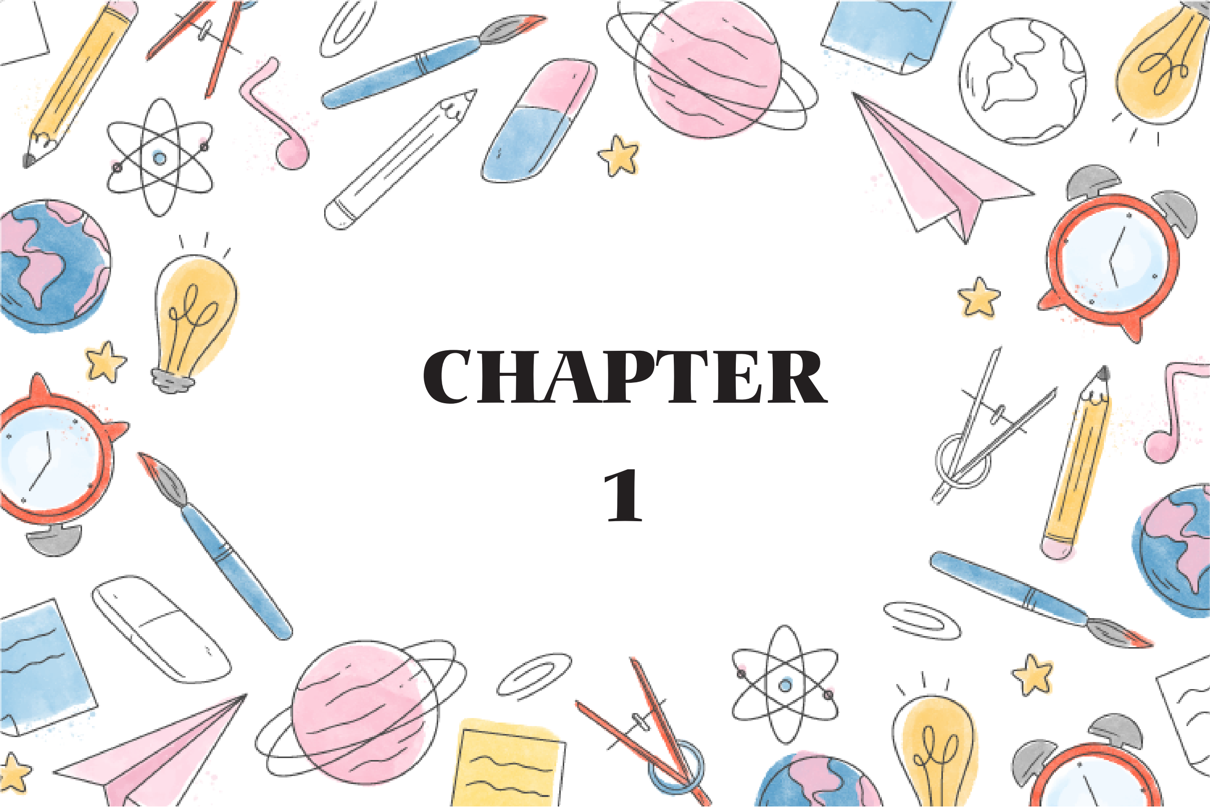

CHAPTER

1

FABRICATION AND CHARACTERIZATION OF METAL-POLYMER-SEMICONDUCTOR SCHOTTKY BARRIER DIODE USING A PTB7:F4-TCNQ INTERFACE LAYER AT DIFFERENT TEMPERATURES

Hüseyin Muzaffer ŞAĞBAN[1]

Özge TÜZÜN ÖZMEN[2]

---

[1] Asst.Prof. H. Muzaffer ŞAĞBAN Opticianry, Vocational School, İstanbul Beykent Üniversitesi, 34500, İstanbul, TURKEY, huseyinsagban@beykent.edu.tr, https://orcid.org/0000-0001-8820-5622

[2] Prof.Dr. Özge TÜZÜN ÖZMEN,Fundamental Sciences, İzmir Bakırçay Üniversitesi, 35665, İzmir, TURKEY, ozge.ozmen@bakircay.edu.tr, https://orcid.org/0000-0002-5204-3737

1. Introduction

Inorganic materials are widely employed in electronic and optoelectronic applications, such as light-emitting diodes (LEDs), silicon-based field-effect transistors (FETs), and thin-film transistors (TFTs) [1]. However, organic electronic devices offer notable advantages over their inorganic counterparts, driven by several intrinsic properties [2]. The primary appeal of organic materials in semiconductor technologies lies in their ease of synthesis using a variety of techniques, coupled with their compatibility with simple production methods such as spin coating and spray deposition. These manufacturing capabilities not only facilitate accelerated research and development but also contribute to a reduction in production costs. Furthermore, organic semiconductors exhibit substantial versatility, as material properties such as molecular weight, bandgap energy, molecular orbital energy levels, structural configuration, and doping can be tailored [3,4]. This adaptability enables the efficient and cost-effective production of organic semiconductor materials with a wide range of customized properties. As a result, organic materials have become increasingly prominent in modern optoelectronic and electronic technologies. Among the most notable organic devices are organic light-emitting diodes (OLEDs), organic field-effect transistors (OFETs), organic photodiodes (OPDs), organic photovoltaics (OPVs), and Schottky barrier diodes (SBDs) [3].

Diodes are among the most essential components in contemporary electronic devices. Of all diode types, Schottky barrier diodes (SBDs) are of particular significance due to their superior performance and capacity to function effectively at high frequencies [5]. Diodes designed for high-frequency applications often struggle to respond to voltage fluctuations, thereby failing to switch between conducting and insulating states efficiently. SBDs, on the other hand, excel in this regard by providing rapid response times even in high-frequency environments. Additionally, SBDs have the advantage of entering the conducting state much faster, as they require a lower forward voltage. Moreover, their reduced number of minority charge carriers leads to lower leakage currents, enhancing their efficiency relative to other diode types. With advancements in organic technology, it has now become possible to fabricate SBDs using organic materials, enabling them to achieve high-performance characteristics as well [6].

The structure of Schottky barrier diodes (SBDs) is typically formed by metal-semiconductor (MS) contacts, with the diode's characteristics influenced by factors such as the type and concentration of the semiconductor, the bandgap, and the metal's work function. SBDs can also be constructed by inserting an insulating or polymeric layer between the metal and semiconductor surfaces, resulting in metal-insulator-semiconductor (MIS) or metal-polymer-semiconductor (MPS) structures. Recently, there has been significant attention paid to experimental and theoretical studies on MPS-type SBDs, especially those incorporating a polymer layer between the metal and semiconductor [2].

MPS-type Schottky barrier diodes (SBDs) are fabricated by depositing a polymer layer on a semiconductor substrate through techniques such as spin coating or spray coating, followed by contact deposition on the front and back surfaces of the structure (Figure 1.1). The inclusion of a polymer with a high dielectric constant between the metal and semiconductor layers allows for the regulation of charge transfer, leading to the production of higher-performance devices. The interfacial layers serve crucial functions, including surface passivation, optimization of the current-conduction mechanism, and reduction of leakage currents. Metals with appropriate work functions are employed to establish rectifying and ohmic contacts during the preparation of MPS-type structures. For metal/n-type semiconductor contacts, a rectifying contact occurs when the metal work function (Φm) exceeds the semiconductor work function (Φs), while an ohmic contact is formed when Φs > Φm. Similarly, for metal/p-type semiconductor contacts, a rectifying contact occurs when Φs > Φm and an ohmic contact is formed when Φm > Φs [7-13].

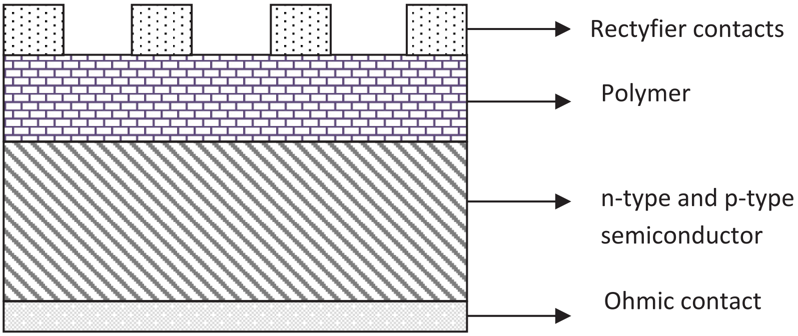

Figure1.1. Schematic Representation of an MPS Schottky Barrier Diode

In the present study, the fabrication and electrical characterization of MPS-type Schottky barrier diodes (SBDs) were explored, taking into account the advantages outlined above. For this purpose, PTB7 (Poly({4,8-bis[(2-ethylhexyl)oxy]benzo[1,2-b:4,5-b′]dithiophene-2,6-diyl}{3-fluoro-2-[(2-ethylhexyl)carbonyl]thieno[3,4-b]thiophenediyl})) was used as the primary material, with F4-TCNQ (2,3,5,6-Tetrafluoro-2,5-cyclohexadiene-1,4-diylidene)dimalononitrile, 7,7,8,8-Tetracyano-2,3,5,6-tetrafluoroquinodimethane) employed as the doping agent. SBDs were fabricated by preparing mixtures with a doping ratio of 1% PTB7 to F4-TCNQ.

2. Materials and Methods

In this investigation, n-type doped silicon (Si) crystals were employed as the semiconductor material. The organic polymer layer was applied to the n-type Si substrate using the spin coating technique (Figure 1.2). Following the deposition of the polymer/semiconductor material, Schottky barrier diodes (SBDs) were fabricated by depositing metal contacts on the top and bottom of the structure through a thermal evaporation system. Gold (Au) and silver (Ag) metals were selected for the contacts due to their appropriate work functions relative to the doping type of the materials utilized.

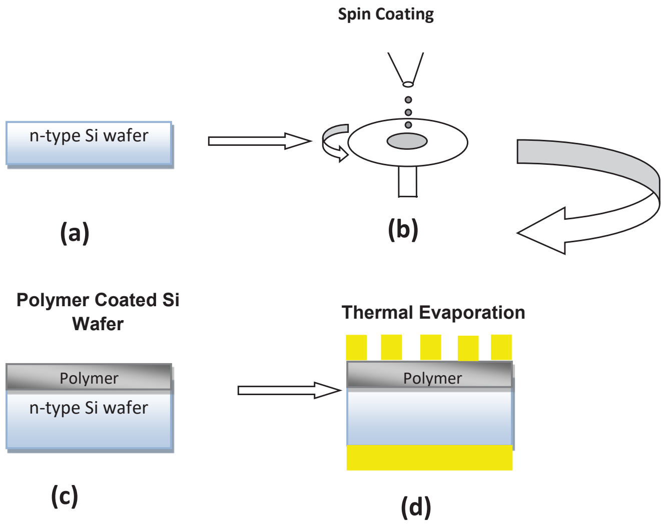

Figure1.2. Stages of the Fabrication Process for MPY Schottky Barrier Diodes

The n-type single-crystal Si wafers used as substrates were fabricated using the Czochralski (Cz) method with a <100> crystallographic orientation. The Si wafers, intended for SBD fabrication, were procured with a thickness of 350 ± 25 µm and a resistivity of 4.8 Ω·cm. These wafers were cut into 1x1 cm squares using a diamond saw. The wafers were then cleaned, and a high-purity Ag layer, approximately 2500 Å thick, was deposited on the matte side of the wafers using a thermal evaporation system and a mask, forming ohmic contacts. The organic materials, PTB7 and F4-TCNQ, were used as the interfacial layer and were mixed in chlorobenzene at concentrations of 20 mg/ml and 0.01 mg/ml, respectively. This mixture was stirred at 60°C for about 3 hours, after which it was placed in a tube with a 1% F4-TCNQ doping ratio and stirred for 24 hours. The resulting solution was then spin-coated onto the shiny side of the Si wafers for 30 seconds at 1500 rpm, achieving a layer thickness of approximately 160 nm. Finally, rectifying contacts were deposited onto the coated organic layers using the thermal evaporation method, with high-purity Au being used to create a contact layer approximately 2500 Å in thickness.

The electrical properties of the fabricated SBDs were analyzed through measurements conducted both in the dark and under illumination. These measurements were carried out in a closed-circuit cryostat at a vacuum of 1x10^-4 mbar and over a voltage range of -5V to +5V. Illumination experiments were conducted with a light intensity of 1000 W/m². Temperature-dependent current-voltage (I-V) measurements of the SBDs were performed over a temperature range of 200K to 325K in 25K increments. From the I-V measurements conducted under dark, illuminated, and temperature-variable conditions, the ideality factors, saturation currents, and barrier heights of the SBDs were extracted.

3. Results and Discussion

The electrical properties of Schottky barrier diodes (SBDs) fabricated with a 1% doping ratio of PTB7:F4-TCNQ polymer blend were analyzed under both illumination and varying temperatures. Initially, current-voltage (I-V) measurements were performed for the Au/PTB7:F4-TCNQ/n-Si heterojunction SBD at room temperature under vacuum. Subsequently, temperature-dependent I-V measurements were conducted within a vacuum at temperatures ranging from 200K to 325K in 25K increments. From these measurements, key electrical parameters such as the ideality factor (n), saturation current (I_0), and barrier height ($\emptyset_B$) were calculated to characterize the behavior of the fabricated SBDs.

Dark and illuminated I-V measurements of the Au/PTB7:F4-TCNQ/n-Si SBD were carried out in a closed-circuit cryostat, under a pressure of approximately 1x10^{-4} mbar, over a voltage range of -5V to +5V in the dark, and under an illumination of 1000 W/m^2. Figure 3.1 illustrates the I-V curves of the diode under both dark and illuminated conditions with a 1% PTB7:F4-TCNQ doping ratio.

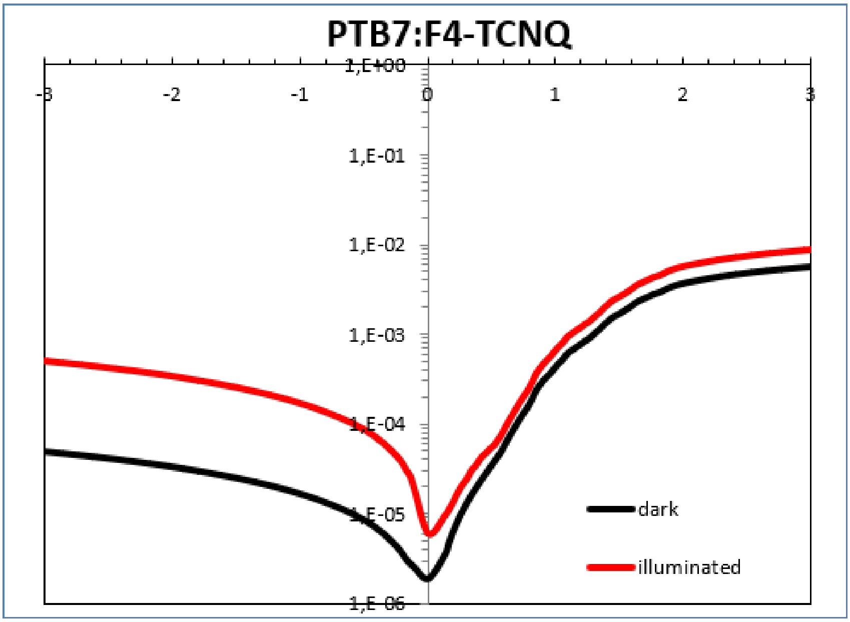

Figure3.1: Dark and Illuminated I-V Characteristics of the Heterojunction SBD with 1% PTB7:F4-TCNQ Doping Ratio

In Figure 3.1, it is observed that the current increases in both the negative and positive regions when the diode is exposed to light. This increase can be attributed to the generation of additional electron-hole pairs upon exposure to light, which enhances charge carrier movement in the diode [16]. Moreover, the increase in conductivity under illumination is also due to the excitation of trap levels within the bandgap, which contributes to the conduction process [17]. The enhancement of conductivity is particularly noticeable in the negative region, where minority charge carriers generated by the light significantly affect conduction under reverse bias. This behavior suggests that the SBD exhibits photodiode-like characteristics under illumination.

The ideality factor (n), barrier height ($\emptyset_B$), and saturation current (I_0) of the SBDs were calculated using standard equations. The ideality factor was determined from the slope of the linear region of the I-V characteristics, following the equation [3]:

$$n = \frac{q}{kT\tan\theta} \tag{3.1}$$

Using this equation, the ideality factor for the diode with a 1% PTB7:F4-TCNQ doping ratio was found to be 3.88 in the dark and 5.36 under illumination. The ideality factor increases under illumination, indicating a deviation from ideal diode behavior.

The barrier height ($\emptyset_B$) was calculated using the following equation:

$$\emptyset_B = \frac{kT}{q}\ln\left(\frac{AA^*T^2}{I_o}\right) \tag{3.2}$$

In this equation, I_o represents the saturation current, which is the current value at zero voltage. For the SBD with 1% PTB7:F4-TCNQ doping, the saturation current was found to be 1.46×10^{-6} A in the dark and 5.17×10^{-6} A under illumination. The barrier height ($\emptyset_B$) was calculated from these saturation current values, yielding a value of 0.75 eV in the dark and 0.71 eV under illumination. These results are summarized in Table 3.1.

Table3.1. The values of ideality factor (n), saturation current (Io), and barrier height ($\emptyset_B$) obtained for the SBD with 1% PTB7:F4-TCNQ doping under dark and illuminated conditions.

	Dark			Illuminated		
	n	$I_o(A)$	$\emptyset_B(eV)$	n	$I_o(A)$	$\emptyset_B(eV)$
PTB7:F4-TCNQ	3.88	1.46×10^{-6}	0.75	5.36	5.17×10^{-6}	0.71

As seen in Table 3.1, the ideality factor and saturation current increase under illumination, while the barrier height decreases slightly. The increase in saturation current is attributed to the enhanced generation of charge carriers under light exposure, which contributes to conduction through quantum tunneling mechanisms. This phenomenon, coupled with the greater energy of charge carriers, leads to the observed increase in the ideality factor and the slight reduction in barrier height. These observations are linked to the reconfiguration of charge carriers under illumination, the interface state density, and the non-uniform distribution of barrier heights in the structure [1, 18].

The rectification ratio (RR) of the SBD was calculated by comparing the forward current to the reverse current at +3V and -3V bias voltages. For the SBD with 1% PTB7:F4-TCNQ doping, the rectification ratio was determined to be 1.15×10^{2}.

Figure 3.2 illustrates the I-V characteristics of the 1% PTB7:F4-TCNQ-doped SBD across the temperature range from 200K to 325K.

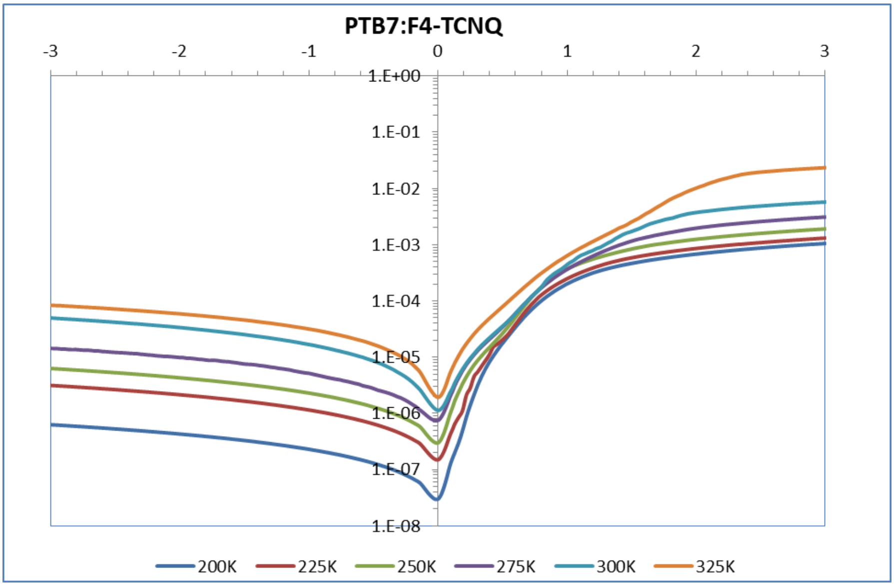

Figure3.2: Temperature-dependent I-V characteristics of the heterojunction SBD with 1% PTB7:F4-TCNQ doping.

From the I-V curves measured at 25K temperature intervals within the range of 200K to 325K, the ideality factors, barrier heights, and saturation currents were determined. The results are summarized in Table 3.2.

Table3.2 Values obtained from the temperature-dependent I-V curves of the diode with a 1% PTB7:F4-TCNQ doping ratio.

PTB7:F4-TCNQ	**200**	**225**	**250**	**275**	**300**	**325**
n	5.04	4.59	4.38	4.10	3.88	3.56
$\emptyset_B$(eV)	0.55	0.59	0.64	0.69	0.75	0.80
Io(A)	3.36 x10^{-8}	1.56 x10^{-7}	3.17 x10^{-7}	7.41 x10^{-7}	1.46 x10^{-6}	2.12 x10^{-6}

An analysis of the data in Table 3.2 reveals that with increasing temperature, the ideality factor decreases, while both the barrier height and saturation current increase. Specifically, for the SBD with a 1% PTB7:F4-TCNQ doping ratio, the ideality factor decreases from 5.04 to 3.56, the barrier height increases from 0.55 eV to 0.80 eV, and the saturation current increases from 3.36×10^{-8} A to 2.12×10^{-6} A.

Figure 3.3 shows the variation of ideality factors and barrier heights with temperature for the SBD with 1% PTB7:F4-TCNQ doping.

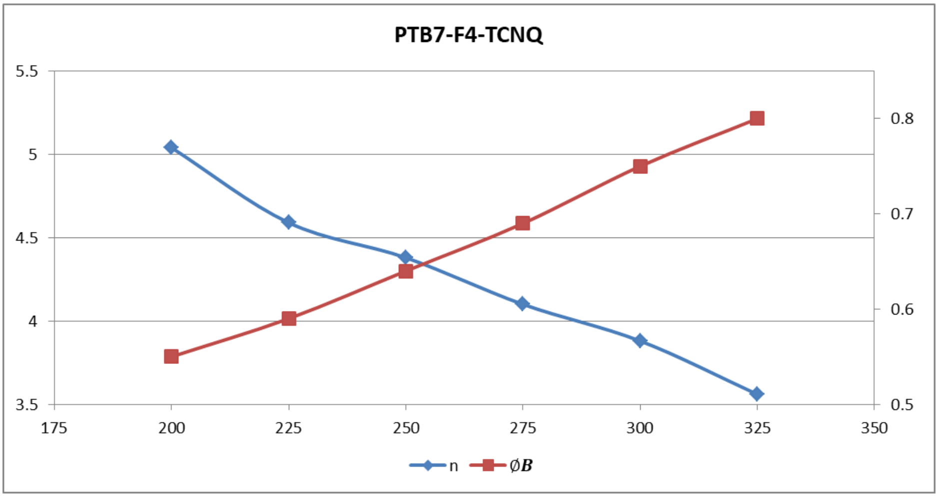

Figure3.3. Temperature-dependent variation in the ideality factor and barrier height for the diode fabricated with a 1% PTB7:F4-TCNQ doping ratio.

As temperature increases, the ideality factor of the diode decreases, while the barrier height increases, which is consistent with previous literature [19, 20]. This temperature-dependent behavior suggests that thermionic emission is not the only mechanism controlling current transport. At lower temperatures, charge carriers have insufficient energy to overcome higher potential barriers, leading to localized current conduction and a higher ideality factor. Additionally, recombination rates are reduced at lower temperatures, leading to lower current values. However, as the temperature increases, charge carriers gain more energy, allowing them to surmount higher potential barriers, which results in a decrease in the ideality factor and an increase in current.

4. Conclusion

This study involved the fabrication of an Au/PTB7:F4-TCNQ/n-Si Schottky Barrier Diode (SBD) with a 1% doping ratio of PTB7:F4-TCNQ. The electrical characteristics of the fabricated SBD were initially measured using current-voltage (I-V) measurements in a closed-circuit cryostat under a vacuum of 1×10^{-4} mbar. These measurements were conducted under both dark and illuminated conditions (1000 W/m^2) across a voltage range of -5V to +5V. Following this, temperature-dependent I-V measurements were performed under the same vacuum conditions, with temperatures ranging from 200K to 325K, also spanning a voltage range of -5V to +5V.

The I-V measurements in both dark and illuminated conditions revealed an increase in current in both reverse and forward bias under light exposure. This increase can be attributed to several factors, including the generation of additional electron-hole pairs due to illumination, the contribution of charge carriers from the forbidden energy gap to the conduction process, and the reduction in the series resistance of the diode due to the presence of light.

Furthermore, temperature-dependent measurements showed that both reverse and forward bias current values increased as the temperature rose. Additionally, an increase in temperature resulted in a decrease in ideality factors and an increase in barrier heights. This behavior can be attributed to the fact that at lower temperatures, charge carriers possess less energy, which limits their ability to overcome the potential barrier. This, in turn, leads to deviations from ideal diode behavior.

5. Acknowledgement

This work was supported by the Düzce University Scientific Research Projects (Project No: BAP 2017.05.02.525).

REFERENCES

[1] Sze S.M., Ng K.K., “Physics of Semiconductor Devices”, 3rd Ed., John Wiley & Sons, Hoboken, New Jersey **(2007).**

[2] Gaojie Lu, “Organic semiconductor”*, University of Rochester* **(2006).**

[3] Tüzün Özmen Ö., “Effects of PCBM concentration on the electrical properties of the Au/P3HT:PCBM/n-Si (MPS) Schottky barrier diodes”, *Microelectronics Reliability,* 54 **(2014)** 2766–2774.

[4] So F., “Organic Electronics; Materials, Processing, Devices and Applications”, *CRC Press*, *Boca Raton*. (**2010**).

[5] R. Hackam, P. Piarrop., “Electrical Properties of Nickel-LowcDoped n-Type Gallium Arsenide Schottky-Barrier Diodes”, *IEEE Transactions On Electron Devices*, ED-19, No. 12 **(1972)** 1231-1238

[6] S. Demirezen, Z. Sönmez, U. Aydemir, S. Altındal.,” Effect of series resistance and interface states on the IeV, CeV and G/ueV characteristics in Au/Bi-doped polyvinyl alcohol (PVA)/n-Si Schottky barrier diodes at room temperature”, *Current Applied Physics,* 12 **(2012)** 266-272.

[7] Li S.S., “Semiconductor Physical Electronics”*,* 2nd Ed., Springer, **(2006)**

[8] Rhoderick E.H., Williams R.H., “Surfaces, Interfaces and Schottky Barriers, Metal-Semiconductor Contacts”, 2nd Ed., *Clarendon Press, Oxford,* **(1988)**.

[9] Wilson A. H., *Proc. R. Soc. Lond. A,* 133 (**1931)** 458.

[10] Sharma B.L., “Metal-Semiconductor Contacts Schottky Barrier Junctions and Their Applications”, *Plenum Press, New York and London*, **(1984)**.

[11] Özdemir A.F., Aldemir D.A., Kökçe A., Altındal S., *Synthetic Metals*, 159 **(2009)** 1427.

[12] Demirezen S., Altındal Ş., *Current Applied Physics*, 10 **(2010)** 1188.

[13] Rhoderick E.H., Williams R.H., “Metal-Semiconductor Contacts”, 2nd Ed., Oxford *University Press, Oxford*, **(1988)**.

[14] Liu J., Shao S., Fang G., Meng B., Xie Z., Wang L.,” High-Efficiency Inverted Polymer Solar Cells with Transparent and Work-Function Tunable MoO_3-Al Composite Film as Cathode Buffer Layer”, *Adv. Mater.* 24 **(2012)**, 2774–2779.

[15] Han X., Wu Z., Sun B., *Organic Electronics*, 14 **(2013)** 1116.

[16] Taşçıoğlu İ., Aydemir U., Altındal Ş., Tunç T., “Illumination dependent admittance characteristics of Au/Zinc Acetate doped Polyvinyl Alcohol (PVA: Zn)/n-Si Schottky Barrier Diodes (SBDs)”, *International Congress On Advances In Applied Physics and Materials Science*, c. 1400, (**2011**) ss. 307-311.

[17] Alialy S., Tecimer H., Uslu H., Altındal Ş., “A comparative study on electrical characteristics of Au/n-Si Schottky Diodes with and without Bi-doped PVA

interfacial layer in dark and under illumination at room temperature", *Journal of Nanomedicine and Nanotechnology,* c. 4, sayı. 3, (**2013**), 1000167.

[18] Altındal Yerişkin S., Uslu H., Tunç T., Altındal Ş., "Illumination effect on admittance measurements of Polyvinyl Alcohol (Co, Zn - Doped)/n - Si Schottky Barrier Diodes in wide frequency and applied bias voltage range", *International Advances in Applied Physics and Materials Science Congress & Exhibition,* , c.1400, (**2011**), ss. 541-545.

[19] Card H.C ve Rhoderick E.H., "Studies of tunnel MOS diodes I. Interface effects in silicon Schottky diodes*", Journal of Physics D: Applied Physics,* c. 4, (**1971**), ss.1589-1601.

[20] R.T. Tung, "Comment on Numerical study of electrical transport in homogeneous Schottky diodes" *Journal of Applied Physics*, c. 88, sayı 3, (**2000**), ss. 7366-7368.

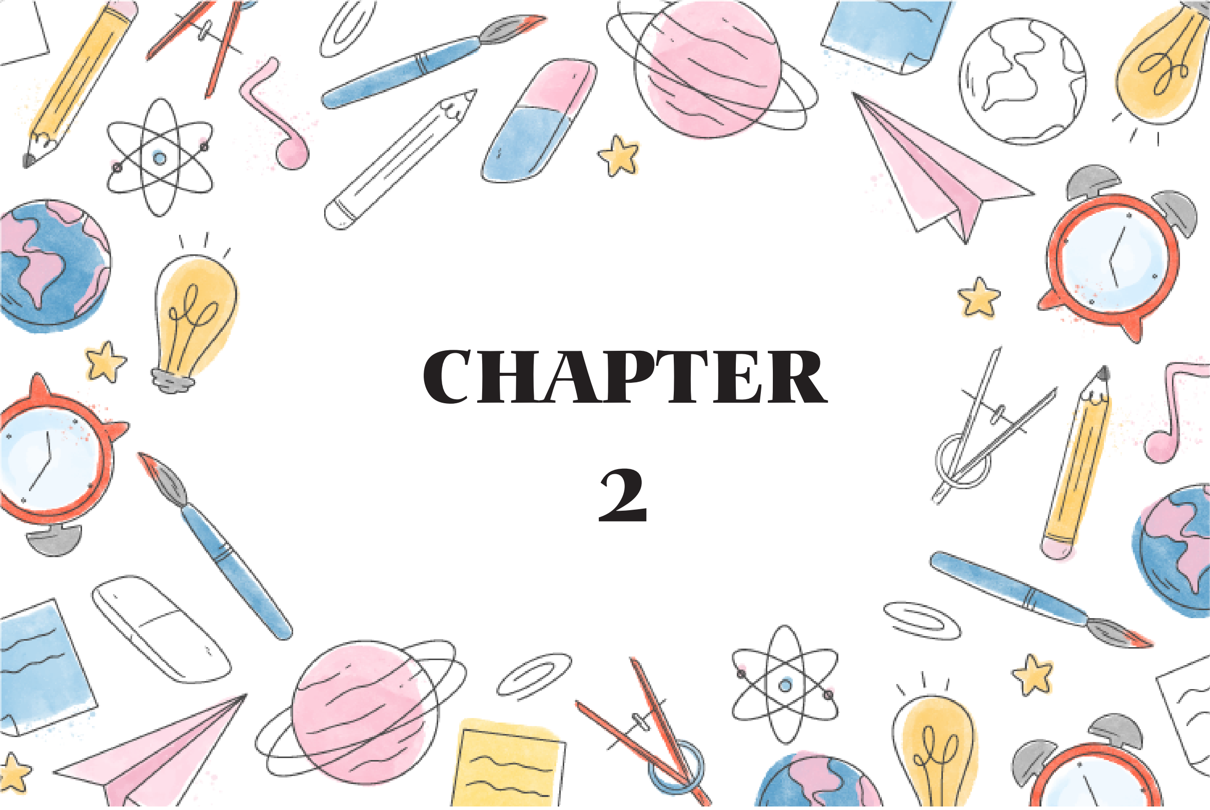

CHAPTER

2

ILLUMINATING NUCLEOSYNTHESIS PROCESSES THROUGH ASTROPHYSICAL S-FACTOR CALCULATIONS[1]

Ercan YILDIZ[2]

---

[1] This article was produced from Ercan Yıldız's doctoral thesis numbered 444309, prepared in 2016 under the supervision of Prof. Dr. Abdullah Aydın.

[2] Ercan Yıldız , orcid:0000-0001-8709-4764

Kahramanmaras Sutcu Imam University, Vocational School of Health Services

Dept. of Medical Imaging Tech., Kahramanmaras, Turkey

1. Introduction

When energetic particles (such as neutrons, protons, or electrons) possess sufficient kinetic energy, they can interact with and approach target nuclei, potentially being captured by them. Experimental data have shown that despite their electric charge, particles can approach nuclei closely enough for nuclear forces to dominate and enable such fusion events (Arya, 1966). This indicates that short-range attractive nuclear forces become dominant at very close distances between the projectile and the nucleus.

Immediately after a particle is captured by a nucleus—typically within less than 10^{-13} seconds—the system reorganizes itself by emitting either a gamma ray or a particle different from the incoming one. This process is defined as a **nuclear reaction**. The newly formed nucleus may be stable or unstable; if unstable, it undergoes decay in accordance with the laws of radioactivity over a characteristic half-life. As a result, the nucleus obtained after the reaction generally has different atomic and mass numbers than the initial target nucleus.

Studies of nuclear reactions play a fundamental role in understanding the structural properties of the nucleus, such as its size, charge distribution, and the nature of nuclear forces. Therefore, nuclear reactions are of great importance not only for applied research but also for fundamental physics. Each nuclear reaction, much like a chemical reaction, can be represented by a reaction equation (Arya, 1966):

$$a + X \rightarrow \boldsymbol{C^*} \rightarrow Y + b \qquad (1.1)$$

Where:

- a: Incident (projectile) particle,
- X: Target nucleus,
- C*: Compound nucleus formed at the intermediate stage,
- Y and b: Reaction products.

The incoming and outgoing particles are usually nucleons (protons, neutrons) or light nuclei; in some cases, photons may also participate in the reaction. This reaction can also be represented in the alternative form **X(a,b)Y**.

Reactions can be classified based on the outgoing particles:

- If **a = b** and **Y = X**, the reaction is an **elastic scattering**.
- If **a = b** but **Y ≠ X**, meaning the target is left in an excited state, it is termed **inelastic scattering**.
- If the outgoing particles differ from the incoming ones, the reaction is considered a **transformation reaction**.

In this context, the compound nucleus **C*** is formed by the complete fusion of the projectile and the target nucleus. It decays within a very short time (about 10^{-16} seconds) by emitting one or more particles and produces the reaction products.

1.2 Cross Section and Nuclear Reactions

In the study of nuclear reactions and scattering events, a quantitative measure is required to express the likelihood of a specific reaction occurring. For this purpose, one of the fundamental concepts used in nuclear physics is the **cross section**, which quantitatively defines the probability of a particular nuclear reaction taking place. It is one of the key quantities employed in the analysis of nuclear interactions and can be directly measured experimentally (Satchler, 1990).

The cross section expresses the interaction probability in terms of an effective area and is typically measured in **barns**, where (1 barn = 10^{-24} cm^2) This allows for the quantitative analysis of processes at microscopic scales. Thanks to the cross section concept:

- Different types of reactions can be compared,
- Energy-dependent behavior of nuclear reactions can be analyzed,

- The consistency between theoretical models and experimental data can be evaluated.

$$\sigma = \frac{\text{Number of b particles emitted}}{\text{(The number of a particles passing through a unit surface)(Number of target cores)}} = \frac{N_b}{I_0 N} \quad (1.2)$$

1.3. The Big Bang and Evolutionary Process

The question of how the universe came into existence has long intrigued scientists, leading to the development of various theories. Studies on the origin of the universe have not only aimed to explain this process but have also raised new fundamental questions.

The development of element synthesis theories dates back to the 1920s. In 1920, Aston expressed the relative masses of hydrogen and helium atoms; shortly after, Eddington proposed that the Sun's energy could be generated through the hydrogen-helium conversion, known as the **proton-proton chain**. However, Eddington realized that the Sun’s temperature was insufficient to initiate this conversion and was unable to explain the source of the required energy.

It has since been suggested that nuclear synthesis began with the Big Bang, and through fusion reactions in the expanding and cooling universe, light elements such as ^{1}H, ^{4}He, and ^{7}Li were formed. In the following phases, stars began to form, and nucleosynthesis processes commenced within these stellar interiors. Elements up to iron were produced via nuclear burning reactions in stars, whereas elements heavier than iron could only be synthesized in high-energy explosive environments such as supernovae.

The formation mechanisms during such explosive events are categorized into:

- the s-process and r-process, which lead to the production of neutron-rich isotopes,
- and the p-process, responsible for proton-rich isotopes.

Elements located in the neutron-rich region of the isotope chart are synthesized via slow (s) and rapid (r) neutron capture processes, while those in the proton-rich region are formed through the p-process. A schematic representation of the Nucleosynthesis Theory explaining the origin of elements is shown in Figure 1.1.

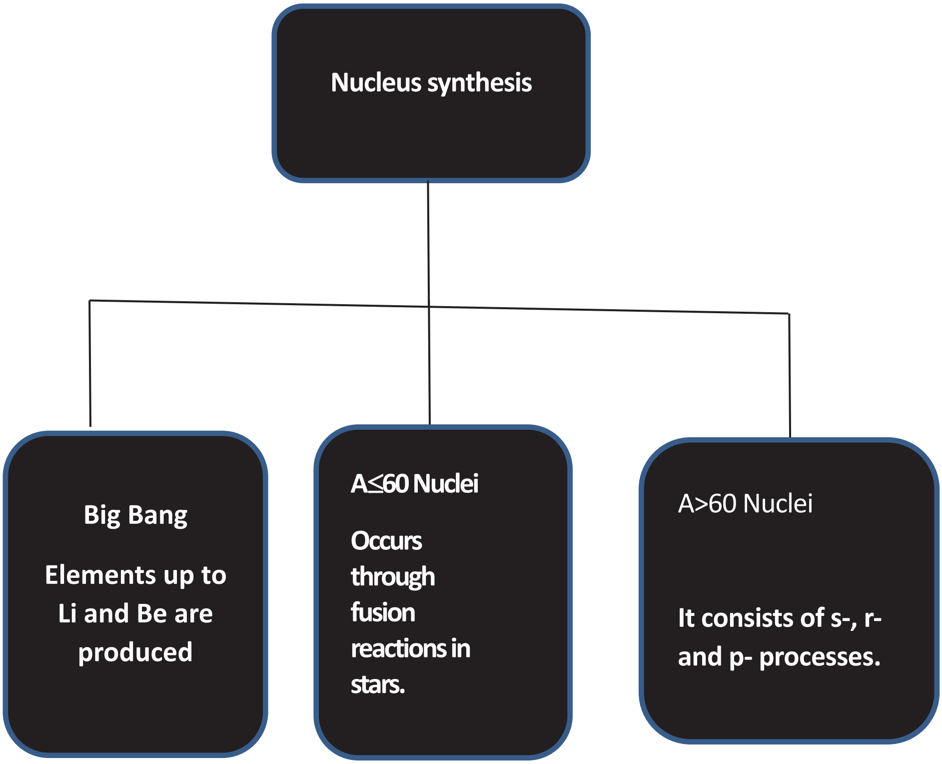

Figure 1.1. Nucleosynthesis Theory

1.4 Big Bang Nucleosynthesis

Big Bang nucleosynthesis refers to the formation of light nuclei such as hydrogen (^{1}H), its isotope deuterium (^{2}H), helium isotopes (^{3}He and ^{4}He), and lithium isotope (^{7}Li) in the very early universe, shortly after the Big Bang, according to the standard cosmological model. As a result of this process, the distribution of visible matter in the universe by mass is approximately:

- 75% hydrogen (^{1}H),
- 25% helium (^{4}He),

- with trace amounts (~0.01%) of deuterium (^2H),
- and even smaller amounts of lithium and beryllium.

It is important to note that nuclei heavier than beryllium are not formed during Big Bang nucleosynthesis. This process was not a localized event; it occurred uniformly and simultaneously throughout the entire universe (Yalçın, 2010).

Synthesis of Nuclei with A < 60

The formation of stars begins with the gravitational collapse of a gas cloud composed primarily of hydrogen and helium. During this collapse, the gravitational potential energy of the atoms is converted into kinetic energy, increasing the temperature of the environment. Once the temperature becomes sufficiently high, protons can overcome their mutual Coulomb repulsion, initiating nuclear fusion processes.

Stellar nucleosynthesis starts with the production of light elements and progresses through a series of fusion reactions that lead to the formation of heavier nuclei. As massive stars approach the **supernova phase**, they develop an **onion-like layered internal structure**. Each layer, from the surface to the core, hosts different fusion reactions, resulting in the formation of progressively heavier elements (Korkulu, 2014). While lighter elements such as hydrogen are found in the outer layers, heavier elements are synthesized in the inner layers during later stages of stellar evolution.

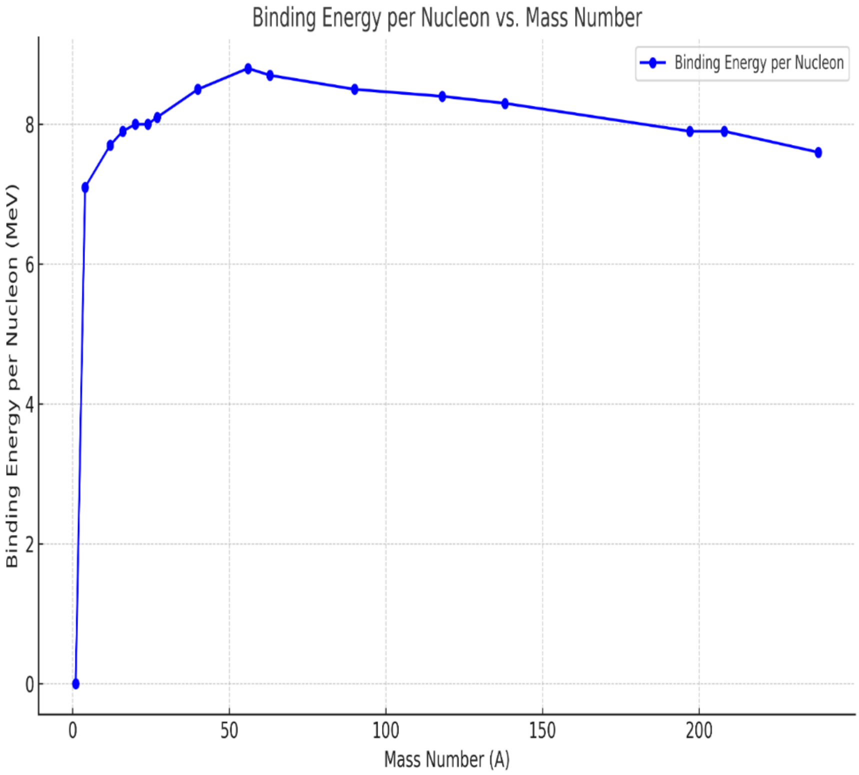

Figure 1.2. Binding energy change per nucleon according to mass number.

The pre-supernova star exhibits an **onion-like layered structure**. Beginning with an outermost layer composed of hydrogen, progressively deeper layers contain heavier elements that were synthesized through successive fusion reactions during the star's lifetime (Korkulu, 2014). These layers are schematically illustrated in **Figure 1.3**.

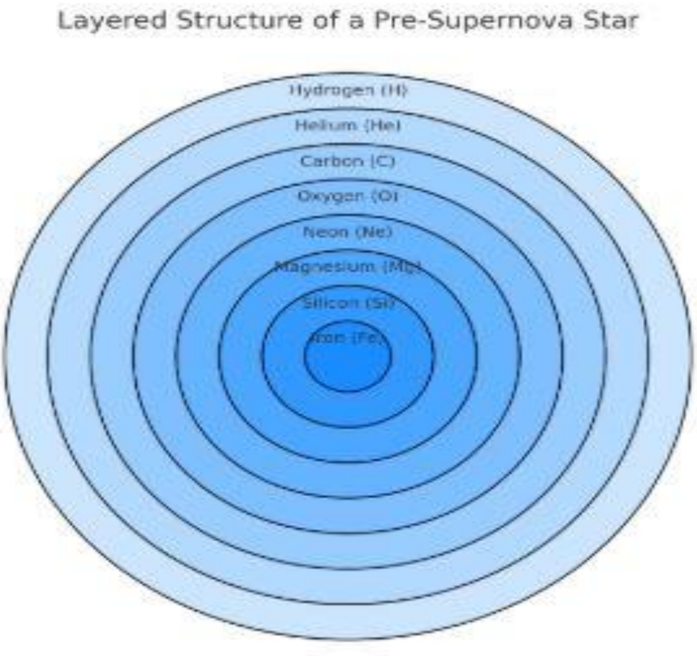

Figure 1.3. Schematic representation of the state of a massive star before a supernova explosion.

Synthesis of Nuclei with A > 60

The synthesis of nearly all nuclei heavier than iron (Fe) is primarily governed by two neutron capture processes: the **s-process** (slow neutron capture) and the **r-process** (rapid neutron capture) (Hampel, Stancliffe, Lugaro, and Meyer, 2016). These processes occur under different astrophysical conditions, determined mainly by the timescale of neutron capture relative to β-decay. A smaller number of rare isotopes, which cannot be explained by these two processes, are believed to be formed through a third mechanism known as the **p-process** (proton capture or photodisintegration).

- s-process (slow neutron capture): A process in which neutrons are captured slowly compared to β-decay, typically occurring under low neutron fluxes and over long timescales. It is predominantly observed in Asymptotic Giant Branch (AGB) stars.

- r-process (rapid neutron capture): This process occurs in environments with high neutron flux, where neutron captures happen faster than β-decay. Supernova explosions and neutron star mergers are considered as primary sites for the r-process.
- **p-process (proton capture / photodisintegration):** This process accounts for the production of proton-rich rare isotopes that cannot be formed via s- or r-processes. It is generally thought to occur under high-temperature conditions, where gamma rays induce photodisintegration reactions.

An analysis of the elemental abundance distribution in the Solar System suggests that these three processes operate under distinct timescales, temperatures, and neutron densities, and that these varying conditions collectively shape the synthesis of heavy elements.

Astrophysical S-Factor and Cross Section

The **cross section (σ)** is a fundamental quantity that determines the probability of a nuclear reaction occurring and is strongly energy-dependent. In reactions involving charged particles, the likelihood of interaction depends on several factors: the relative energy of the particles, the nuclear structure of the reactants, and the height of the Coulomb barrier.

If the reaction energy corresponds to an excited state of the compound nucleus, a **resonance** occurs, leading to a sharp increase in the cross section. In the absence of such a resonance, the process is classified as **non-resonant**.

In non-resonant reactions involving charged particles, the cross section at low energies primarily depends on two key factors:

1. **Coulomb tunneling probability (P):** The quantum mechanical probability that a charged particle can tunnel through the Coulomb barrier.
2. **Energy-dependent attenuation term (1/E):** Reflects the variation in reaction probability with energy.

Under these considerations, the nuclear reaction cross section can generally be expressed as:

$$\sigma(E)=S(E).E\cdot\exp(-2\pi\eta)\ ,\ S(E)=\sigma(E)\ .\ E.\ \exp(2\pi\eta)\quad (MeV.b)$$
(1.3)

$$S(E)=\sigma(E)\ .\ E.\ \exp(31{,}29.\ Z_1.\ Z_2.\ \mu^{1/2}.\ E^{-1/2})\quad (MeV.b)$$
(1.4)

Here, η is the **Sommerfeld parameter**, defined by the expression: $(Z_1Z_2e^2)/\hbar\upsilon$, Z_1 and Z_2 are the charges of the interacting nuclei 1 and 2. μ represents the reduced mass. Since the **astrophysical S-factor**, S(E), varies much more slowly with energy compared to the cross section σ(E), it offers significant theoretical advantages—especially in the low-energy domain where direct measurement of the cross section is technically challenging or even impossible. In such cases, extrapolating the function S(E) to lower energies allows for meaningful theoretical interpretation and prediction (Yildiz and Aydin, 2016a, 2016b; Yıldız, 2016; YILDIZ and SARPÜN, 2020).

Understanding the nucleosynthesis process requires not only accurate knowledge of nuclear physical parameters but also a proper interpretation of the physical conditions within stellar environments. Expanding these analyses in future studies will enable more precise modeling of reaction networks and allow for a more accurate assessment of the effects of astrophysical parameters such as neutron sources, explosion energies, and types of stars. At the same time, new-generation experimental devices will facilitate more precise measurements of low-energy reactions, thereby providing a stronger foundation for semi-empirical approaches.

In conclusion, the concept of the astrophysical S-factor is regarded not only as a reaction parameter but also as a key that sheds light on the chemical history of the universe. In this context, a deep understanding of nuclear reactions holds the potential to produce more definitive and holistic answers to fundamental questions about the evolution of the universe.

References

Arya, P. A. (1966). *Fundamentals of Nuclear Physics*. Allyn and Bacon.

Hampel, M., Stancliffe, R. J., Lugaro, M., and Meyer, B. S. (2016). the Intermediate Neutron-Capture Process and Carbon-Enhanced Metal-Poor Stars. *The Astrophysical Journal*, *831*(2), 171. https://doi.org/10.3847/0004-637x/831/2/171

Korkulu, Z. (2014). *Karakteristik Gama ve X ışınları ile Reaksiyon Tesir Kesiti ölçümleri*. Kocaeli Üniversitesi Fen Bilimleri Enstitüsü, Kocaeli.

Satchler, G. R. (1990). *Introduction to Nuclear Reactions*. Oxford University Press; 2nd edition (October 18, 1990).

Yalçın, C. (2010). *In-113'ün Alfa Yakalama Reaksiyonu ve Nükleer Astrofizikteki Yeri*. Kocaeli Üniversitesi Fen Bilimleri Enstitüsü, Kocaeli.

Yildiz, E., and Aydin, A. (2016a). Calculation of Cross-sections and Astrophysical S-Factors for 62Ni(α,n) and 62Ni(α,γ) Reactions of Structural Fusion Material Nickel. *Journal of Fusion Energy*, *35*(3), 605–607. https://doi.org/10.1007/s10894-016-0079-9

Yildiz, E., and Aydin, A. (2016b). Calculation of Cross-sections and Astrophysical S-Factors for 62Ni(α,n) and 62Ni(α,γ) Reactions of Structural Fusion Material Nickel. *Journal of Fusion Energy*, *35*(3), 605–607. https://doi.org/10.1007/s10894-016-0079-9

Yıldız, E. (2016). *(a,n) NÜKLEER REAKSİYONLARI İÇİN YARI-AMPİRİK ASTROFİZİKSEL S-FAKTÖR FORMÜLLERİNİN GELİŞTİRİLMESİ*. Kırıkkale Üniversitesi Fen Bilimleri Enstitüsü, Kırıkkale.

YILDIZ, E., and SARPÜN, İ. H. (2020). CALCULATION OF CROSS SECTIONS AND ASTROPHYSICAL S-FACTORS AT 0-5 MeV ENERGY RANGE FOR 8Li (α, n)11B REACTION. *Eskişehir Technical University Journal of Science and Technology A - Applied Sciences and Engineering*, *21*(1), 205–209. https://doi.org/10.18038/estubtda.632019

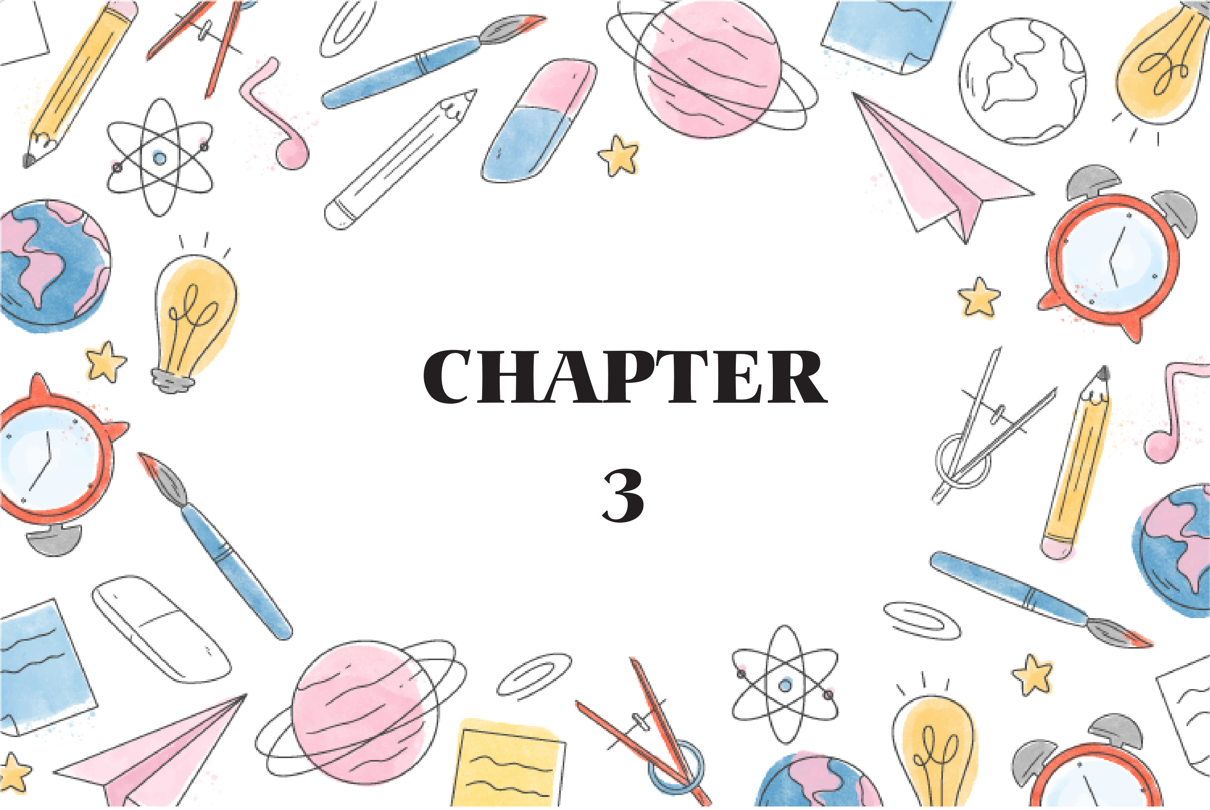

CHAPTER
3

BLAZARS

Prof. Dr. E. Nihal ERCAN

A summary

Blazars have inspired the astrophysics and astronomy community for decades. Due to their energetic structure and orientation toward Earth, they serve as natural laboratories for studying high-energy processes in physics. A notable example occurred on September 22, 2017, when the IceCube telescope in Antarctica detected a high-energy neutrino (~290 TeV). IceCube promptly alerted telescopes worldwide to search for the source of this event, leading instruments such as Fermi-LAT and MAGIC to trace the origin to an active blazar designated TXS 0506+056, located approximately 4 billion light-years away. We believe that events like this foster strong collaboration between the astrophysics/astronomy community and the particle physics community, which ultimately contributes to the growth of the field of Astroparticle physics.

1. Introduction

What is a Blazar?

Blazars are a subtype of Active Galactic Nuclei (AGN) distinguished by the orientation of their jets pointed towards Earth. They represent the most extreme members of the AGN family and are known for being stable and powerful sources of high-energy gamma rays. (Ajello, 2009)

Blazars can be divided into two categories: BL Lacertae objects (commonly referred to as BL Lacs) and Flat Spectrum Radio Quasars (FSRQs). The primary differences between these two classes lie in their emission lines. BL Lacs typically exhibit weak or undetectable emission lines, whereas FSRQs showcase very pronounced emission lines. The unification of blazars remains a persistent challenge in the study of Active Galactic Nuclei. (Prandini, 2022)

Blazars are a type of radio-loud Active Galactic Nuclei (AGNs) characterised by their polarised, bright, and rapidly fluctuating non-thermal continuum emissions, spanning from radio waves to gamma rays (in GeV and TeV ranges), originating from a relativistic jet that is nearly aligned with the observer's line of sight. Consequently, they serve as uncommon environments for investigating the physics and structure of extragalactic jets found in all radio-loud AGNs. (Sambruna, 2000)

Blazars are typically very variable objects, exhibiting changes that can occur over timescales from months to mere minutes. The intricacy of the spectral energy distribution (SED) varies based on the classification of the objects, with FSRQs displaying a generally more complex SED accompanied by multiple overlapping contributions. (Prandini, 2022)

When was it discovered?

The history of blazars is closely tied to the discovery of the first quasar. This quasar, identified as 3C 272, was discovered in 1963 and is also recognised as the first blazar ever detected. Meanwhile, 3C 373 was a radio source that exhibited visual correspondence, and spectroscopic analysis confirmed its extragalactic nature.

Nearly six decades after the initial identifications, thousands of blazars now populate the extragalactic sky. Just 20 years ago, before the publication of the 2019 source, only a few hundred blazars were known. (Prandini, 2022) Observational advances have played a significant role in enhancing our understanding of blazars and their role in the high-energy universe. The EGRET (Energetic Gamma Ray Experiment Telescope) telescope has identified 271 point sources emitting over 100 MeV, which are included in the third EGRET (3EG) catalogue and consist of active galactic nuclei (AGNs). Among these, EGRET has identified 46 blazars exhibiting emissions greater than 100 MeV, demonstrating their significant activity. (Böttcher, 2007)

Other Active Galactic Nuclei

AGN constitute a large fraction of the high-energy gamma-ray sources in the known universe, accounting for about 61.4% of the 5,064 gamma-ray sources in the most recently completed Fermi-LAT 4FGL catalogue. In addition to blazars, misaligned AGN or point-like objects such as radio galaxies and Narrow-Line Seyfert 1 galaxies also play an important role in understanding the high-energy universe. (Gamble Jr, 2024)

Blazar Sequences

The blazar sequence is a concept that describes how the observed spectral energy distributions (SEDs) of blazars vary with their luminosity. It suggests that different types of blazars—Flat Spectrum Radio Quasars (FSRQs) and BL Lacertae objects (BL Lacs)—form a continuous sequence, rather than being fundamentally distinct classes. (Cha, 2014)

The original version of the blazar sequence was proposed by Fossati et al. (1998). Using multiwavelength data from 126 sources, including gamma-ray observations above 30 MeV from the EGRET satellite, Fossati identified systematic trends in the SEDs of blazars. This study showed that more luminous blazars (typically FSRQs) tend to have SED peaks—

both synchrotron and inverse Compton—at lower frequencies, while less luminous blazars (usually BL Lacs) peak at higher frequencies.

With the discovery of ~1,500 blazars by the Fermi-LAT satellite, Ghisellini et al. (2017) introduced a refined version known as the Fermi blazar sequence. This updated sequence focused on gamma-ray SEDs (in the MeV–GeV range), ranking blazars by their brightness and analysing patterns in their emission.

A key insight from the Fermi blazar sequence is the connection between luminosity, peak frequency, and the Eddington ratio. While early interpretations emphasised radiative cooling as the main factor shaping the sequence, Ghisellini proposed that the Eddington ratio—the ratio of a blazar's accretion rate to the Eddington limit—is the dominant physical driver. In this framework, FSRQs have high Eddington ratios and more radiatively efficient accretion disks, leading to greater luminosity and lower-frequency SED peaks. Conversely, BL Lacs, particularly High-energy BL Lacs (HBLs), have lower Eddington ratios, weaker emission lines, and higher-frequency peaks.

Although the blazar sequence provides a useful unifying framework, its physical basis remains debated. Some argue it reflects selection effects or environmental differences rather than a true evolutionary or physical sequence. (Prandini, 2022)

2. Observational Properties of Blazars

The emission characteristics of blazars fluctuate across all wavelengths. These fluctuations occur over a wide range of time scales, from minutes to hours (intra-day variability), weeks to months (short-term variability), and months to years (long-term variability).

They are recognised for exhibiting two prominent broad spectral features: the initial peak arises from synchrotron radiation, while the second bump is likely due to inverse-Compton emission that is prevalent in leptonic models. In hadronic models, proton-synchrotron emission and pion/muon cascades can significantly contribute.

The intense emission they produce between the radio and visual bands is highly polarised. Features like high polarisation, rapid variability, and compact radio cores have resulted in these AGN types being generally classified as blazars. (Gamble Jr, 2024)

Blazars are celestial bodies that are a special type of active galactic nuclei (AGN) and are quite rare in the universe. Blazars make up only 10-15%

of "radio noisy" active galaxies. Of all active galaxies (Seyfert galaxies, quasars, radio galaxies, etc.), blazars represent a much smaller fraction. Therefore, the observed blazars are also rare.

In addition to the few introductory observational properties mentioned above, I will share one artist's depiction and two observed photos of Blazars to create a vivid image of Blazars in your minds.

Figure 1 – Blazar Artist Concept
Credit: NASA. (n.d.). *Blazar Artist Concept* [Illustration]. NASA Image and Video Library. https://images.nasa.gov/details/PIA20912

The illustration above depicts a blazar with a supermassive black hole at its centre. As matter spirals around and into the black hole, it emits light and can form jets of particles that travel at nearly the speed of light. The white jet visible on the right side of the portrayal is what defines a blazar. When this jet is directed toward Earth, the galaxy appears exceptionally bright across various wavelengths and is classified as a blazar.

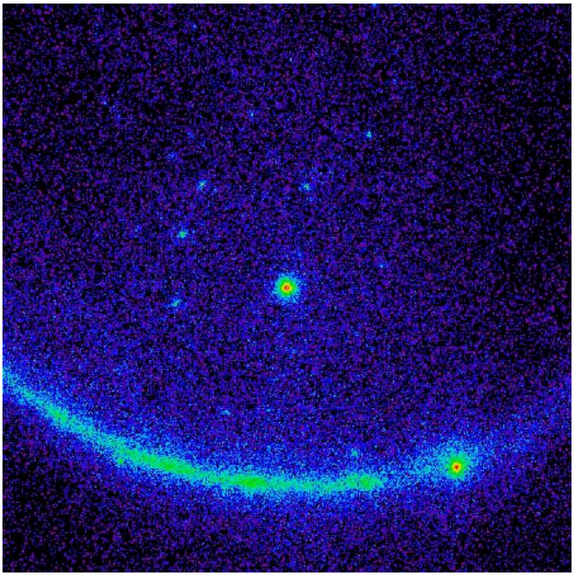

Figure 2 – Fermi Sports a Record Flare from Blazar
Credit: NASA. (n.d.). *Fermi Sports a Record Flare from Blazar* [Illustration]. NASA Image and Video Library. https://images.nasa.gov/details/fermi-spots-a-record-flare-from-blazar_19578977022_o

The second figure presents a representation of a massive gamma-ray flare from the blazar 3C 279, which was captured by NASA's Fermi Gamma-ray Space Telescope. In 2025, 3C 279 produced a flare that made it the brightest gamma-ray source in the sky, even exceeding the brightness of the Vela pulsar. What made this flare particularly unique was its rapid variability; its brightness changed dramatically over just a few hours, indicating that the gamma-ray emitting region is compact, likely smaller than the distance between the Earth and the Sun.

The highest-energy gamma ray detected during this flare was 52 GeV (giga electronvolts), which is incredibly energetic. This event suggests highly efficient acceleration mechanisms, possibly involving magnetic reconnection, where magnetic field lines rapidly rearrange and release energy.

This flare poses a challenge to existing models of jet physics. The fact that such high energies were reached in such a small region over such short timescales compels theorists to refine their understanding of black hole jet dynamics and radiation processes, such as synchrotron emission and inverse Compton scattering.

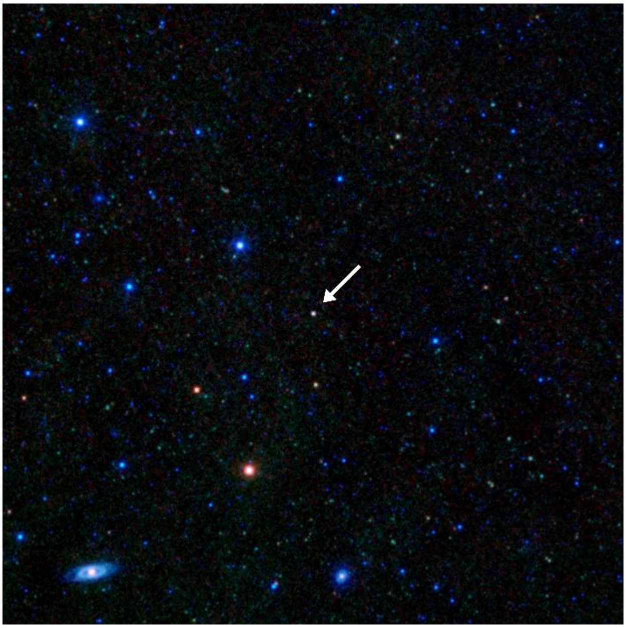

Figure 3 – Lone Blazar

Credit: NASA. (n.d.). *Lone Blazar* [Illustration]. NASA Image and Video Library. https://images.nasa.gov/details/PIA15424

This figure is remarkable even by its standards. In the image, a single white dot stands out, indicating that it is bright across all four bands. This dot represents the blazar located right at the centre.

The image is an infrared composite captured by the WISE (Wide-field Infrared Survey Explorer) satellite. Although WISE was not specifically designed to detect blazars, as it was a general all-sky infrared mission, researchers have discovered that blazars have a unique infrared signature due to synchrotron radiation emitted from their jets.

Astronomers compared known gamma-ray sources identified by the Fermi telescope with infrared sources from WISE. They observed that some infrared objects had no optical or radio counterparts but matched the energy profiles of known blazars.

This blazar is one such match—it had previously gone unidentified in other wavelengths but has now been confirmed. This detection demonstrates that WISE can assist in identifying unknown blazars. Additionally, it suggests that many unassociated gamma-ray sources catalogued by Fermi might be blazars that have not been recognised due to being optically faint or obscured. These findings advance efforts to create a more complete catalogue of blazars.

After reviewing these examples, readers should have a clearer understanding of how a Blazar appears. Therefore, we can proceed with the theoretical aspects of Blazars.

3. Theoretical Aspects of Blazars

3.1 Formation of Jets and Plasma Physics

A. Formation of Jets

The formation processes of relativistic jets continue to be a major area of research in astrophysics, with the theoretical understanding of their development posing unresolved challenges. A key model in this field is the Blandford-Znajek (BZ) mechanism, which describes how energy is extracted from rotating black holes through the twisting of magnetic field lines. This process leads to outflows that are primarily dominated by Poynting flux and are aligned with the black hole's rotation axis. (Gamble Jr, 2024)

The luminosity associated with the BZ mechanism is influenced by both the spin parameter of the black hole and the intensity of the magnetic field. Recent simulations and observations utilising magnetohydrodynamics (MHD) and general relativistic magnetohydrodynamics (GRMHD) have suggested that the main contribution to jet outflows stems from poloidal magnetic field configurations around relativistic matter accreting onto the central object.

A significant challenge remains in the limited understanding of the fundamental mechanisms that initiate these jets, particularly whether they are dominated by Poynting flux or are magnetohydrodynamic. There are still open questions regarding how jets become populated with particles and how relativistic particles, characterised by Lorentz factors exceeding 10, accelerate to ultra-relativistic speeds. (Gamble Jr, 2024)

B. Plasma Aspect

Blazar jets exhibit non-thermal emissions that range from radio waves to high-energy gamma rays and even cosmic rays. The detected radiation is likely produced by a relativistic jet oriented at a small angle relative to our line of sight.

These jets consist of a relativistic plasma made up of ultra-relativistic electrons and/or pairs (in leptonic models), as well as relativistic protons and secondary particles like muons, mesons, and neutrons (in hadronic models). Research indicates a growing body of evidence suggesting that the jets may be energetically and dynamically dominated by their proton content, even though the pairs of particles may outnumber the protons. (Böttcher, 2007)

It is believed that these jets contain relativistic particles that can flow in a continuous stream or appear in discrete "blobs." The particles present in the plasma generate non-thermal radiation, with the main radiation mechanisms being the synchrotron process for low-energy emissions and Inverse Compton (IC) scattering for high-energy emissions.

Synchrotron emission occurs when relativistic electrons travel through magnetic fields within the jet, contributing to the low-frequency portion of the spectral energy distributions (SED). IC scattering can take two forms: "synchronous self-Compton" (SSC), where electrons scatter their synchrotron photons, and "external Compton" (EC), where they scatter external photons from sources like the accretion disk, broad-line region (BLR), or dust torus. (Sambruna, 2000)

In hadronic models, ultra-relativistic protons can interact with primary protons, leading to the production of secondary muons and mesons through synchrotron radiation or the creation of pions. (Böttcher, 2007)

3.2 Emission Mechanisms

Blazars are a type of Active Galactic Nuclei (AGN) that exhibit significant emission across the entire electromagnetic spectrum, ranging from radio waves to high-energy gamma rays. This radiation is believed to originate from relativistic jets launched by supermassive black holes, which are aligned closely with our line of sight. The emission from these jets primarily arises from non-thermal processes.

The Spectral Energy Distributions (SEDs) of blazars typically display two broad and distinct peaks. These peaks can be explained by non-thermal radiation mechanisms driven by relativistic particles—primarily electrons, but potentially also protons and electron-positron pairs—within the jet. (Böttcher, 2007)

A. Main Emission Mechanisms

Two main emission mechanisms are widely accepted in blazar theory:

1. Synchrotron Radiation: The first, low-energy peak in the SED is the result of synchrotron emission by relativistic electrons spiralling in the magnetic fields of the jet. The power of synchrotron radiation depends on several parameters, including the magnetic field strength (B), the Lorentz factor of the particles (γ), and the pitch angle (α) between the particle velocity and the magnetic field lines. Magnetic fields are crucial not only for the emission process but also for governing the efficiency of particle acceleration within the jet. (Gamble Jr, 2024)

2. Inverse Compton (IC) Scattering: The second, high-energy peak in the SED arises from inverse Compton scattering, where relativistic electrons transfer energy to low-energy photons, boosting them to higher energies. There are two main types of IC processes:

a) Synchrotron Self-Compton (SSC): In this mechanism, electrons scatter the synchrotron photons that they have emitted themselves. This process is particularly relevant in environments with weak external photon fields, such as with some BL Lacertae objects. (Gamble Jr, 2024)

b) External Compton (EC): In this case, electrons scatter external photons originating from regions outside the jet. These external photons may come from the accretion disk, the Broad Line Region (BLR), or a surrounding dusty torus. EC is especially effective in explaining high-energy emissions in blazars that have strong external radiation fields, such as Flat Spectrum Radio Quasars (FSRQs). (Cha, 2014)

B. Hadronic Models

In addition to leptonic (electron-based) scenarios, hadronic models have been proposed to explain high-energy emissions by incorporating relativistic protons and their interactions. In these models, ultra-relativistic protons may emit synchrotron radiation or interact with photons (e.g., through pion interactions or photomeson production), leading to the creation of secondary particles such as pions and muons. The decay and radiation of these secondary particles can also contribute to the observed gamma-ray emissions.

One notable model, called the hadronic synchrotron mirror model, suggests that protons interact with synchrotron photons reflected off surrounding structures, producing gamma rays. There is growing evidence that the jets may be energetically and dynamically dominated by protons, even though electron-positron pairs might still outnumber protons in terms of particle count. (Böttcher, 2007)

3.3 Time Variations

We discussed the variability of timescales of Blazars in the Introduction part, yet although we are going to repeat some of the things from there, I believe the variability of Blazars carry unique features that we should know if we want to learn about Blazars.

Blazars exhibit significant variability, and their emissions are known to fluctuate over a wide range of timescales, from minutes to years, making them key targets in the field of time-domain astrophysics. These fluctuations are generally categorised into three main types based on their duration: intraday, short-term, and long-term variability. (Gamble Jr, 2024)

Intraday variability (IDV), also referred to as microvariability, occurs over timescales of minutes to hours and indicates very compact emission regions. Observations of blazars such as Mrk 421 have demonstrated flux changes in the TeV energy range that can last as briefly as 15 minutes. Likewise, Mrk 501 has shown that flux can double within approximately 30 minutes in the TeV bands. In PKS 2155–304, linked flares between optical and X-ray bands have been observed on timescales of hours. Notably, X-ray data sometimes reveal that higher photon energies can lead to lower energies by up to an hour, suggesting intricate particle cooling and acceleration mechanisms. (Sambruna, 2000)

Short-term variability occurs over several days to a few months and is often related to dynamics within the jet or shock wave propagation. For instance, the blazar PKS 1622–297 has demonstrated rapid variability on day-long scales. These outbursts may result from transient phenomena such as magnetic reconnection or instabilities occurring within the jet. (Sambruna, 2000)

Long-term variability, which is noticeable over periods of months to years, is associated with broader changes in the structure of the jet or the central accretion process. In quasars (QSOs), it is common to observe changes exceeding 10% for a year, and in optically violent variable (OVV) quasars, flux can double in the same timeframe or vary by 0.1 magnitudes within just a few nights. The historical light curve of 3C 279 from 1991 to 1998 exemplifies classic long-term variability, and multi-epoch spectral energy distributions (SEDs) of these blazars demonstrate clear spectral changes over time. (Wiita, 2006)

It's important to note that blazar variability encompasses not just flux changes but also notable variations in the spectrum. For instance, in Mrk

501, the spectral index has been documented to fluctuate between 1.89 and 2.72, while in Mrk 421, flaring events have shown spectral hardening at X-ray energies. Alterations in the gamma-ray spectrum could indicate changes in the distribution of relativistic electrons or the seed photon population involved in inverse Compton scattering. Monitoring these spectral variations on short timescales is vital for understanding particle acceleration and cooling processes. (Mukherjee, 2003)

Certain BL Lac objects demonstrate X-ray variability patterns referred to as spectral hysteresis, where changes in spectral hardness either lag behind or precede flux variations. This has been interpreted as an indication of ultrarelativistic electrons being gradually injected or accelerated into the jet, followed by a period of synchrotron cooling. In PKS 2155–304, analyses of hardness–intensity diagrams in the X-ray band have shown both clockwise and counterclockwise hysteresis loops during distinct flares, serving as a diagnostic for the relative timescales of acceleration and cooling. Rapid flux and spectral variability are also observed in optical bands, frequently accompanied by spectral hardening during flare events. (Sambruna, 2000)

These rapid and varied fluctuations strongly suggest that energy release occurs over very compact scales close to the central engine of the host galaxy. Since the timescale of variability correlates with the light-travel time across the emitting region, these findings enable astrophysicists to explore extremely small physical areas within the jet or disk.

Variability across multiple wavelengths—especially when correlated across different energy bands—offers essential constraints for emission models. This approach provides a means to evaluate cooling theories by comparing observed time delays and amplitudes to theoretical expectations. In homogeneous models, a single population of electrons generates both synchrotron (low-energy) and inverse Compton (high-energy) emissions, resulting in concurrent variability without significant time lags. This behaviour has been validated in blue blazars such as Mrk 421 and Mrk 501, where X-ray and TeV gamma-ray light curves display strong correlations and similar flare characteristics. Nevertheless, in Mrk 421, varying e-folding times—about 1 hour for TeV energies and 5 hours for X-rays—indicate that inhomogeneous models might be necessary, potentially involving multiple emission zones. (Mukherjee, 2003)

Connections between radio and gamma-ray variability also offer valuable insights into the structure of jets. For instance, in TXS 0506+056, a delay in radio flaring has been noted following high-energy activity, suggesting that disturbances are propagating outward along the jet. Strong correlations between radio and gamma emissions have also been observed in both FSRQs and BL Lac objects, implying that these emissions likely originate from the same population of relativistic electrons within the jet. (Gamble Jr, 2024)

The intricate nature of blazar variability stems from the complicated structure of the jet and its emission components. Utilising a multi-wavelength observational approach is essential for effectively analysing and understanding the energy fluctuations in blazars from a theoretical perspective.

3.4 Black Hole and Feeding Processes

In our research on the structure known as “Blazars,” it’s important to remember that the central object is always a supermassive black hole, which powers the surrounding Blazars.

One commonly examined mechanism responsible for jet formation in active galactic nuclei is the Blandford–Znajek (BZ) process. This theory explains how a spinning black hole can extract energy by twisting magnetic field lines that are aligned with its rotational axis, leading to outflows dominated by Poynting flux. The effectiveness of jet production in this context is thought to be heavily influenced by the spin of the black hole. Analysing a broad sample of blazars over various luminosities and redshifts can yield important insights into the contributions of black hole spin and accretion processes to jet activity. (Gamble Jr, 2024)

Another method for extracting energy from a rotating black hole is the Penrose process, which involves the generation of escaping helical polar electron-positron jets and is intrinsically linked to the black hole's rotation.

Jets may also be driven by accretion, where matter falling onto the black hole supplies the necessary energy. Some research suggests that BL Lac objects are mainly powered by drawing spin energy from their central supermassive black holes through the BZ mechanism, while flat-spectrum radio quasars (FSRQs) are thought to obtain a larger share of their power from accretion processes. This notion supports the idea of an evolutionary relationship between FSRQs and BL Lacs, where stronger-lined FSRQs might gradually evolve into weaker-lined BL Lacs as their surrounding gas and dust become depleted. The recent identification of "changing-look" blazars—objects that show transitions between FSRQ-like and BL

Lac-like states—further emphasizes the necessity for additional investigations into the dynamic nature of these sources. (Cha, 2014)

Research on blazar evolution utilising Swift's Burst Alert Telescope (BAT) has provided evidence of a strong relationship between accretion and jet activity. The most luminous active galactic nuclei, and consequently the brightest quasars, are typically associated with the most powerful blazars. This pattern is particularly evident at high redshifts, where gas and dust facilitate effective accretion and massive quasars. (Ajello, 2009)

Some models propose that in BL Lacs, the emission zone is positioned closer to the central engine compared to FSRQs. This could account for the observed differences: stronger magnetic fields, reduced Compton dominance, and higher peak frequencies in BL Lacs. At low accretion rates, the flow of material around the black hole may function in an alternative state, such as an advection-dominated accretion flow (ADAF). (Prandini, 2022)

In summary, the variability and emissions observed in blazars are closely connected to relativistic jets generated by complex feeding mechanisms. These mechanisms encompass both accretion from the surrounding disk and the extraction of energy from the rotating black hole. Understanding the roles of accretion and black hole spin is crucial for gaining insight into the nature and evolution of blazars.

3.5 Neutrino Connections

A. Blazars as Neutrino Sources

Observations of neutrinos have created a new opportunity to examine non-thermal processes in astronomical objects. Nevertheless, the specific sources that generate neutrino emissions remain uncertain. A distinctive feature of neutrinos is that, unlike photons or other particles, they are not absorbed when they interact with background photons or matter. This property allows for the detection of neutrinos even from sources situated at great distances. The pattern of the observed arrival directions predominantly indicates an extragalactic origin for these particles. (Gang Cao, 2020)

Potential extragalactic sources for high-energy neutrinos include active galactic nuclei (AGN), gamma-ray bursts (GRBs), and supernovae. Among these, blazars are considered the most likely candidates for neutrino generation due to their prevalence in the extragalactic gamma-ray sky. Blazars, which are a subclass of AGNs, have relativistic jets that point toward Earth, and their gamma-ray emissions imply the acceleration of particles to extremely high energies. (Kohta Murase, 2018)

Neutrinos are generally linked to hadronic processes occurring in the jets of blazars. These processes entail high-energy protons interacting with surrounding matter or photons, leading to the production of charged pions (π^+), which then decay into muons (μ^+) and neutrinos ($\nu\mu$). This cascade also continues with the decay of muons into electrons (e^+) and electron neutrinos (νe), as well as additional muon neutrinos and antineutrinos. The neutrino emissions that result are regarded as a distinctive indication of hadronic interactions within the blazar jets. (Oikonomou, 2022)

B. TXS 0506+056 and the IceCube-170922A Event

In September 2017, the IceCube Neutrino Observatory observed a significant neutrino event, referred to as IceCube-170922A. This event was closely aligned in time and direction with a gamma-ray flare coming from the blazar TXS 0506+056. This correlation provided the first strong evidence indicating that blazars could be sources of astrophysical neutrinos, representing a key advancement in the field of multi-messenger astronomy. (Kohta Murase, 2018)

In response to the neutrino detection, a comprehensive multi-wavelength campaign was initiated to examine TXS 0506+056 across various wavelengths, from radio to gamma rays. This effort resulted in the first identification of this blazar in the very-high-energy gamma-ray spectrum, utilizing the MAGIC Cherenkov telescopes. The correlation between the high-energy neutrino and the gamma-ray flare was determined to have a significance level of 3.5σ, indicating a possible association between the blazar and the neutrino event. This connection provides a valuable opportunity to investigate the relationship between high-energy photons and neutrinos. (Oikonomou, 2022)

Furthermore, an analysis of archived IceCube data uncovered 13 ± 5 low-energy muon neutrino signals from the same area over five months while TXS 0506+056 was not in a flaring state. This finding implies that neutrino emissions during flaring periods (2017) might differ from those during non-flaring times (2014-2015), enhancing our comprehension of blazar variability and the processes involved in neutrino production. (Oikonomou, 2022)

C. Neutrino Production Mechanisms and Models

High-energy neutrinos can be generated through interactions between protons and photons (p - γ), leading to the creation of charged pions. These pions are unstable and transform into stable particles such as electrons, positrons, neutrinos (ν_e, ν_μ), and gamma-ray photons. For instance, a positively charged pion (π^+) converts into a muon (μ^+) and a muon neutrino (ν_μ), which eventually decays into an electron (e^+), an electron neutrino (ν_e), and an antimuon neutrino ($\bar{\nu}_\mu$). This phenomenon is regarded as a key feature of hadronic interactions within blazar jets. (Gang Cao, 2020)

An alternative proposed mechanism is proton-proton (pp) interactions, although these generally necessitate high plasma densities. Such conditions are not anticipated in the environments of BL Lac objects because of their comparatively lower accretion rates. The observed spectrum of neutrinos aligns more closely with p - γ interactions occurring alongside an external radiation field. (Gamble Jr, 2024)

Leptonic-hadronic hybrid models are frequently utilized to investigate the interconnected electromagnetic and neutrino emissions from blazars. These models take into consideration random particle acceleration and integrate all related radiation processes in a self-consistent way. For TXS 0506+056, the electromagnetic and neutrino spectra can be accurately modeled using proton synchrotron and hybrid leptonic-hadronic approaches based on p - γ interactions. (Gang Cao, 2020)

The hybrid leptonic-hadronic model has demonstrated a superior ability to explain the observed X-ray and gamma-ray spectra of TXS 0506+056 when compared to a purely proton synchrotron model. Furthermore, the neutrino spectrum predicted by the hybrid approach closely matches the observed neutrino spectrum more than that of the proton synchrotron model.

If the IceCube-170922A neutrino event is indeed linked to TXS 0506+056, the hybrid leptonic-hadronic model would be the more favored choice. Analyzing the archival neutrino flare from 2014-2015 requires taking into account a very high proton luminosity and significant baryon loading.

The lack of electromagnetic (EM) cascade radiation related to neutrino production can impose stringent constraints on the models, with a single neutrino detection potentially providing stronger limitations than multiple detections. For example, during a six-month flare from TXS 0506+056, the expected maximum number of neutrinos that IceCube might detect is ≤ 0.05, as larger numbers would contradict the observed EM emission. Multi-zone models or scenarios where the EM emission is obscured by matter could alleviate this constraint, just as two-zone models where neutrinos are generated through interactions with external radiation fields, as their related X-ray cascade emission is isotropic. (Gang Cao, 2020)

D. Conclusions and Future Prospects

It is not feasible to place strict limitations on neutrino production models based solely on a single observed neutrino event. To gain insights into the possible physical relationship between neutrinos and gamma-ray emission, more multi-messenger observations are necessary. Searches for time-dependent neutrinos will be essential for evaluating these hypotheses. (Gamble Jr, 2024)

Blazar flares, like the one detected from TXS 0506+056, might account for a minor percentage (≤ 1-10%) of the overall neutrino flux. Intense neutrino flares are probably infrequent occurrences. Even if blazars are confirmed to be sources of neutrinos, they might not be the primary contributors to the total diffuse neutrino background. (Gang Cao, 2020)

Next-generation neutrino observatories, such as IceCube-Gen2 and KM3NeT, will be vital for clarifying the remaining uncertainties and enhancing our comprehension of neutrino production mechanisms in blazars. (Giommi, 2019)

4. Discussion, Conclusion, and Future Aspects

We covered many aspects of the known information about Blazars today and even explored some potential directions for future studies. In this section, I would like to facilitate a discussion and create an overall image to help the reader gain a better understanding of the topic. To achieve this, we will visualize the complete picture of Blazars once more, and for some mental exercise, we will discuss their cooperative positions for future neutrino experiments.

4.1 The full picture of Blazars

Blazars represent a subgroup of radio-loud active galactic nuclei (AGN) that are fueled by supermassive black holes located at the centers of galaxies. Their extreme brightness and variability are thought to stem from a relativistic jet that is closely oriented with our line of sight, resulting in the Doppler boosting of the emitted radiation. Blazars can be primarily divided into two categories: BL Lacertae objects (BL Lacs), which exhibit weak or absent emission lines, and Flat Spectrum Radio Quasars (FSRQs), which show prominent broad emission lines. Their spectral energy distributions (SEDs) display two broad peaks: one low-energy component due to synchrotron radiation and a high-energy component typically ascribed to inverse Compton scattering in leptonic models or proton-related phenomena in hadronic models. (Sambruna, 2000)

These AGNs reveal rapid changes in brightness over a wide range of timescales, from mere minutes to several years, and their emissions cover a spectrum from radio waves to very-high-energy gamma rays. They are important candidates as sources of ultra-high-energy cosmic rays (UHECRs) and high-energy astrophysical neutrinos, with FSRQs being efficient producers of neutrinos and BL Lacs possibly accelerating cosmic-ray nuclei. Observational research, including findings from Swift/BAT and Fermi-LAT, indicates that blazars may follow an evolutionary progression from FSRQs to Low Energy BL Lac objects (LBLs) to High Energy BL Lac objects (HBLs), driven mainly by a reduction in Eddington ratios rather than the mass of the black hole. However, relying solely on spectral data does not fully constrain emission models, and analysing time-resolved spectral variability is deemed essential for resolving ambiguities between competing theories. (Gamble Jr, 2024)

4.2 A brief note for Neutrino Studies

Beyond conventional hadronic models, hybrid leptonic-hadronic frameworks have demonstrated a more effective explanation for both electromagnetic (especially X-ray and gamma-ray) and neutrino spectra of TXS 0506+056. These models incorporate stochastic particle acceleration and all radiative processes in a self-consistent manner. However, as both purely leptonic and hadronic single-zone spectral energy distributions (SEDs) can fit the observations under different parameter assumptions, short-timescale spectral variability is crucial for differentiating between competing models. Some research has also investigated two-zone models to better meet the constraints imposed by electromagnetic cascades. (Gang Cao, 2020)

While blazars can serve as potential point sources of neutrinos during flare events, studies suggest they do not significantly contribute to the diffuse neutrino flux below 100 TeV. Stacking analyses generally provide upper limits on their contribution, which are highly dependent on the assumptions regarding spectral index and energy range. Nevertheless, blazars might still contribute significantly episodically due to their extreme brightness during flares. (Kohta Murase, 2018)

Upcoming neutrino observatories like IceCube-Gen2 and KM3NeT, particularly those with sensitivity to sub-EeV ranges (such as Ashra-NTA, GRAND, POEMMA, RNO-G, Trinity), will play a crucial role in probing diffuse blazar neutrino emissions. Complementary advancements in gamma-ray (LHAASO, CTA), X-ray (eROSITA, Athena), and radio (SKA) instrumentation, along with X-ray polarimetry (IXPE), are important for assembling a comprehensive understanding of blazar physics. The lack of successors for instruments like Fermi-LAT or the rapid-response capabilities of Swift raises concerns regarding potential observational gaps in future studies. Additionally, initiatives like "Open Universe for Blazars" aim to improve the accessibility and usability of multi-frequency datasets, fostering wider participation in multi-messenger astrophysics. (Giommi, 2019)

I would like to thank Mr. Efe Demircan, one of my undergraduate students, for his help in preparing the manuscript.

References:

1. Prandini, E., & Ghisellini, G. (2022). The blazar sequence and its physical understanding. *Galaxies, 10*(1), 35. https://doi.org/10.3390/galaxies10010035
2. Gamble Jr, R., Forman, J., Barnes, A., Srinivasaragavan, G., Holt, I., & Jones Jr, M. (2024). Multi-messenger emission characteristics of blazars. *Frontiers in Astronomy and Space Sciences, 11*, 1401891. https://doi.org/10.3389/fspas.2024.1401891
3. Sambruna, R. M. (2000, June). Understanding blazar jets through their multifrequency emission. In *AIP Conference Proceedings* (Vol. 515, No. 1, pp. 19–30). American Institute of Physics. https://doi.org/10.1063/1.1302776
4. Böttcher, M. (2007). Modeling the emission processes in blazars. In *The Multi-Messenger Approach to High-Energy Gamma-Ray Sources* (pp. 95–104). Springer Netherlands. https://doi.org/10.1007/978-1-4020-6127-0_8
5. Ajello, M., Costamante, L., Sambruna, R. M., Gehrels, N., Chiang, J., Rau, A., ... & Mushotzky, R. F. (2009). The evolution of Swift/BAT blazars and the origin of the MeV background. *The Astrophysical Journal, 699*(1), 603. https://doi.org/10.1088/0004-637X/699/1/603
6. Cha, Y., Zhang, H., Zhang, X., Xiong, D., Li, B., Dong, X., & Li, J. (2014). The evolutionary sequence of Fermi blazars. *Astrophysics and Space Science, 349*, 895–908. https://doi.org/10.1007/s10509-013-1654-6
7. Giommi, P., Brandt, C. H., de Almeida, U. B., Pollock, A. M. T., Arneodo, F., Chang, Y. L., ... & Turriziani, S. (2019). Open Universe for Blazars: A new generation of astronomical products based on 14 years of Swift-XRT data. *Astronomy & Astrophysics, 631*, A116. https://doi.org/10.1051/0004-6361/201936663
8. Mukherjee, R. (2003). Blazars—Observational aspects. *Frontiers Science Series*, 103–112.
9. Oikonomou, F. (2022). High-energy neutrino emission from blazars. *Proceedings of Science (PoS), ICRC2021*, 030. https://doi.org/10.22323/1.395.0030
10. Murase, K., Oikonomou, F., & Petropoulou, M. (2018). Blazar flares as an origin of high-energy cosmic neutrinos? *The Astrophysical Journal, 865*(2), 124. https://doi.org/10.3847/1538-4357/aada00
11. Cao, G., Yang, C., Yang, J., & Wang, J. (2020). A self-consistent leptonic–hadronic interpretation of the electromagnetic and neutrino emissions from blazar TXS 0506+056. *Publications of the Astronomical Society of Japan, 72*(2), 20. https://doi.org/10.1093/pasj/psz142